ADVANCED OPTICAL MATERIALS
www.advopticalmat.de

Switchable Second-Harmonic Generation of Airy Beam and Airy Vortex Beam

Yuan Liu, Wei Chen, Jie Tang, Xiaoyi Xu, Peng Chen, Chao-Qun Ma, Wang Zhang, Bing-Yan Wei, Yang Ming, Guo-Xin Cui, Yong Zhang, Wei Hu, and Yan-Qing Lu**

Airy beam and Airy vortex beam with intriguing characteristics have been extensively studied in linear optics, while their dynamic nonlinear conversion has rarely been explored and remains challenging. Here, through the collaboration of binary mask engineered nonlinear photonic crystal and space-variant liquid-crystal geometric phase element, second-harmonic Airy beam and Airy vortex beam can be generated in a switchable manner. Electrical-controlled loading of orbital angular momentum (OAM) into fundamental wave unlocks the flexibility of nonlinear process, which is well investigated in theory and further verified by experiment. Wavelength transformation, OAM conversion, and propagation trajectory inflection are realized simultaneously. This offers a convenient and universal strategy for dynamic nonlinear generation and shows great potentials in optical manipulation and information processing.

Structured light, as the customized control of amplitude, phase, polarization, and other degree of freedom of light, has become a rapidly advancing topic in these years.[1] Among diverse types, Airy beam, which is described by a wave packet of Airy function,[2] remains invariant during propagation, possesses a constant transversal acceleration and exhibits a self-healing phenomenon.[3–5] Since Airy beam was firstly demonstrated in experiment,[3] these unique properties facilitate its applications in particle manipulation,[6] light bullets,[7] and high-resolution microscopy.[8,9] Furthermore, Airy beam plays a critical role in combination with other structured light. In particular, Airy beam can be embedded with a helical phase-front, contributing to the so-called Airy vortex beam (AVB). Compared with traditional Airy beam, the main lobe of AVB splits because of the carried orbital angular momentum (OAM).[10] Optical vortex in such a hybrid beam is also endowed with unusual propagation dynamics of the curved trajectory.[11–13] Coupled features of Airy beam and OAM bring AVB more possibilities in various cutting-edge areas. Experimentally, there are mainly two approaches to obtain an AVB, where liquid crystal (LC) based spatial light modulator is usually involved. One way is to directly modify the Gaussian beam by encoding a phase singularity into the cubic phase that corresponds to the Fourier transformation of common Airy beam.[14,15] The other is in step by illuminating the prepared vortex beam onto the Airy beam generator, or vice versa.[16]

Most of researches on Airy beam and AVB are under linear optical condition. Moreover, nonlinear process converts structured light to a new wavelength and adds fantastic properties,[17–21] promoting the all-optical manipulation of Airy beam and AVB. Second-harmonic generation (SHG) of one-dimensional (1D) Airy beam was firstly demonstrated during the three-wave mixing processes induced by an asymmetric nonlinear photonic crystal.[22] The caustic and acceleration properties of second-harmonic (SH) Airy beam can be controlled in different nonlinear conditions. The concept of volume holography was further introduced to design the nonlinear optical superlattice for the harmonic generation of 1D Airy beam.[23] Recently, frequency doubling of AVB has been realized as well. By illuminating a spatial light modulator reshaped fundamental wave (FW) onto a homogenous nonlinear medium, the parabolic trajectory of nonlinear circle and ellipse AVBs can be easily adjusted.[24,25] Despite this progress, the dynamic switching and nonlinear conversion between Airy beam and AVB are of great significance, yet still challenging.

In this work, we propose a simple and practical method to realize switchable SHG of Airy beam and AVB through combination of inhomogeneous anisotropic linear media and asymmetrically modified nonlinear photonic crystal. On one hand, an electrical-engineered lithium niobate (LN) crystal with a binary

Y. Liu, Dr. W. Chen, Dr. J. Tang, X. Y. Xu, Dr. P. Chen, C.-Q. Ma, W. Zhang, Dr. Y. Ming, Dr. G.-X. Cui, Prof. Y. Zhang, Prof. W. Hu, Prof. Y.-Q. Lu
National Laboratory of Solid State Microstructures
Key Laboratory of Intelligent Optical Sensing and Manipulation
College of Engineering and Applied Sciences, and Collaborative Innovation Center of Advanced Microstructures
Nanjing University
Nanjing 210093, China
E-mail: chenpeng@nju.edu.cn; yqlu@nju.edu.cn
Dr. B.-Y. Wei
MOE Key Laboratory of Material Physics and Chemistry under Extraordinary Conditions, and Shaanxi Key Laboratory of Optical Information Technology
School of Physical Science and Technology
Northwestern Polytechnical University
Xi'an 710129, China
Dr. Y. Ming
School of Physics and Electronic Engineering
Changshu Institute of Technology
Suzhou 215000, China
The ORCID identification number(s) for the author(s) of this article can be found under https://doi.org/10.1002/adom.202001776.

DOI: 10.1002/adom.202001776

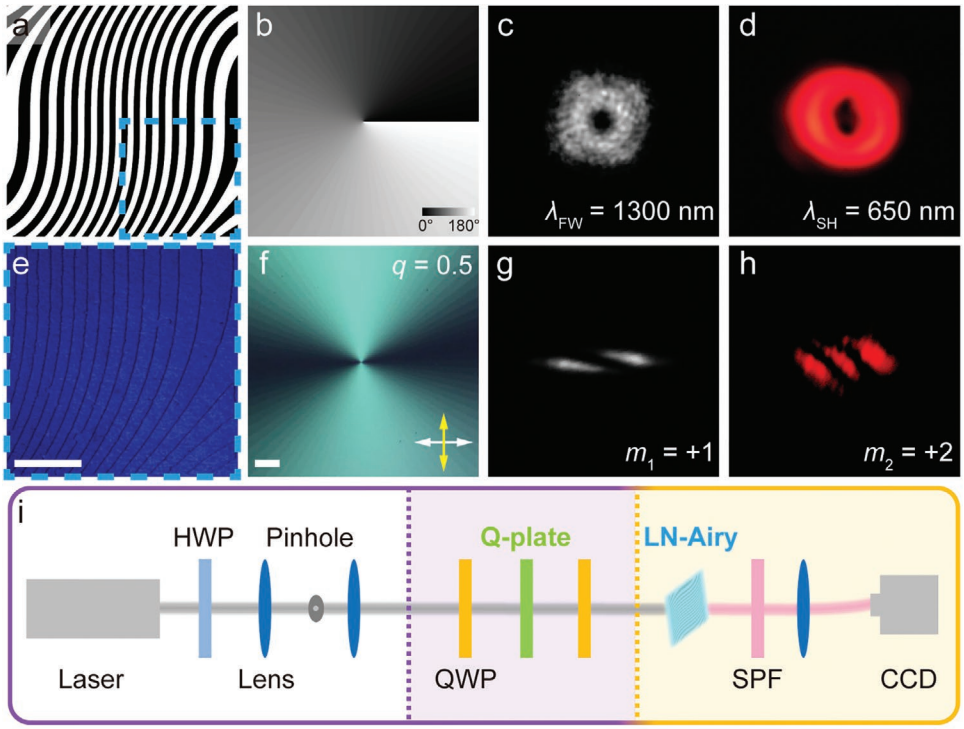

Figure 1. a) Theoretical phase mask to generate second-harmonic (SH) Airy beam with black and white stripes representing 0 and π phase. e) Corresponding SH confocal micrograph of the fabricated lithium niobate (LN) Airy mask. b) Theoretical director distribution and f) polarized micrograph of liquid crystal (LC) q-plate with $q = 0.5$. All scale bars are 100 µm. c,d) Generated optical vortices and g,h) corresponding detection results based on astigmatic transformation of the fundamental wave (FW) ($\lambda_{FW} = 1300$ nm) and SH beam ($\lambda_{SH} = 650$ nm), respectively. i) Schematic of the optical setup. HWP, half-wave plate; QWP, quarter-wave plate; LN-Airy, Airy mask modified LN nonlinear photonic crystal; SPF, short pass filter; CCD, charge coupled device.

pattern encoded quadratic susceptibility is adopted to directly generate a pair of nonlinear two-dimensional (2D) Airy beams. On the other hand, via electrically tuning the photo-patterned LC q-plate with space-variant directors, the OAM loading into the FW can be flexibly controlled. These enable the dynamic switch between Airy beam and AVB in SHG process. The nonlinear OAM conversion and the self-acceleration property of SH AVB are investigated as well. This work provides a novel way to achieve dynamic steering of nonlinear structured light.

To realize the harmonic generation of Airy beam, we use the typical nonlinear crystal LN, whose domains with positive and negative quadratic susceptibility will induce the π phase difference to converted SH waves.[26] Referring to the principle of binary computer-generated holograms,[27] the information of object beam can be stored in a space-dependent binary phase mask, which can be further used to modulate the sign of nonlinear coefficient. Here, a linearly gradient phase integrated cubic phase mask (**Figure 1**a) is designed to transform the Gaussian beam into SH Airy beam in first diffraction orders. The quadratic susceptibility distribution of such a LN-Airy mask can be expressed as:

$$\chi^{(2)}(x,y) = d_{ij}\,\mathrm{sign}\left\{\cos\left[\frac{2\pi x}{\Lambda} + \left(\frac{x^3}{d^3} + \frac{y^3}{d^3}\right)\right]\right\} \tag{1}$$

where d_{ij} is the element of $\chi^{(2)}$ tensor (d_{22} is mainly involved in this process), and d corresponds to the transverse scale of Airy beam and is set as 132 µm. The linearly gradient phase ($2\pi x/\Lambda$, $\Lambda = 33$ µm) is added to provide a reciprocal vector, which can compensate for the transverse phase mismatch. This method is usually adopted in nonlinear beam shaping and contributes to the so-called Raman–Nath diffraction.[17,21]

A switchable LC q-plate is further integrated to realize the dynamic loading of OAM to the FW. Q-plate is a typical geometric phase optical element and can conveniently generate high-quality optical vortex through the spin-to-OAM conversion, which is now widely applied in both classical and quantum optics.[28,29] It possesses space-variant optical axes following $\alpha = q\varphi + \alpha_0$, where q represents the variation frequency, φ is the azimuthal angle, and α_0 is the initial orientation and usually assumed to be zero.[28] Consider a sandwich configuration composed of two quarter-wave plates (QWPs) and one q-plate, the incident y-polarized FW ($\mathbf{E}_0 = E_0 \times [0, 1]^T$) will turn to

$$\begin{aligned}\mathbf{E}_1 &= \mathbf{J}_{QWP}\mathbf{J}_q\mathbf{J}_{QWP}\mathbf{E}_0 \\ &= \frac{1}{\sqrt{2}}\begin{bmatrix}1 & -i\\ -i & 1\end{bmatrix}\cdot\mathbf{R}(-\alpha)\begin{bmatrix}\exp(-i\Gamma/2) & 0\\ 0 & \exp(i\Gamma/2)\end{bmatrix} \\ &\quad \mathbf{R}(\alpha)\cdot\frac{1}{\sqrt{2}}\begin{bmatrix}1 & -i\\ -i & 1\end{bmatrix}\cdot\begin{bmatrix}0\\ 1\end{bmatrix}E_0 \\ &= -iE_0\begin{bmatrix}\cos\dfrac{\Gamma}{2}\\ -\sin\dfrac{\Gamma}{2}\exp(i2q\varphi)\end{bmatrix}\end{aligned} \tag{2}$$

$\Gamma = 2\pi(n_{eff}-n_o)d_{LC}/\lambda$ is the phase retardation of LC q-plate, where n_{eff} changes from n_e to n_o with the applied electric field due to LC molecule tilting.[30] Thus, the FW can be dynamically controlled between optical vortex and Gaussian beam by electrical tuning.

Take $\mathbf{E}_1$ as the pump wave of the LN nonlinear photonic crystal, the evolution of first SH diffraction order during three-wave mixing processes is given by

$$\begin{aligned}\frac{dA_{2x}}{dz} &= -\kappa \exp\left[i2\pi x/\Lambda + i\left(\frac{x^3}{d^3}+\frac{y^3}{d^3}\right)\right]\cdot 2A_{1x}A_{1y} \\ &\quad\times \exp\left[i(2k_1-k_{2z})z - ik_{2x}x\right] \\ &= 2\kappa E_0^2 \cos\frac{\Gamma}{2}\sin\frac{\Gamma}{2}\exp(i2q\varphi) \\ &\quad\times \exp\left[i\left(\frac{x^3}{d^3}+\frac{y^3}{d^3}\right)\right]\cdot \exp\left[i(2k_1-k_{2z})z\right] \\ &\quad\times \exp\left(i2\pi x/\Lambda - ik_{2x}x\right) \\ &= \begin{cases} 0, & \Gamma = (2n+1)\pi \\ 0, & \Gamma = 2n\pi \end{cases}\end{aligned} \tag{3}$$

$$\begin{aligned}\frac{dA_{2y}}{dz} &= \kappa\cdot\exp\left[i2\pi x/\Lambda + i\left(\frac{x^3}{d^3}+\frac{y^3}{d^3}\right)\right]\cdot\left(-A_{1x}^2+A_{1y}^2\right) \\ &\quad\times \exp\left[i(2k_1-k_{2z})z - ik_{2x}x\right] \\ &= \kappa E_0^2\left[-\cos^2\frac{\Gamma}{2}+\sin^2\frac{\Gamma}{2}\exp(i4q\varphi)\right]\cdot\exp\left[i\left(\frac{x^3}{d^3}+\frac{y^3}{d^3}\right)\right] \\ &\quad\times \exp\left[i(2k_1-k_{2z})z\right]\cdot\exp\left(i2\pi x/\Lambda - ik_{2x}x\right) \\ &= \begin{cases} \kappa E_0^2\exp\left[i\left(\frac{x^3}{d^3}+\frac{y^3}{d^3}\right)+i4q\varphi\right]\cdot\exp\left[i(2k_1-k_{2z})z\right] \\ \quad\times\exp\left(i2\pi x/\Lambda - ik_{2x}x\right), \quad \Gamma=(2n+1)\pi \\ -\kappa E_0^2\exp\left[i\left(\frac{x^3}{d^3}+\frac{y^3}{d^3}\right)\right]\cdot\exp\left[i(2k_1-k_{2z})z\right] \\ \quad\times\exp\left(i2\pi x/\Lambda - ik_{2x}x\right), \quad \Gamma=2n\pi \end{cases}\end{aligned} \tag{4}$$

κ is the nonlinear coupling coefficient. A_1, A_2 and k_1, k_2 are the amplitude and wave-vector of the FW and SH beam, respectively. In this Raman–Nath diffraction, the transverse phase matching condition is satisfied in the first order, i.e., $k_{2x} = 2\pi/\Lambda$, thus the right component in Equation (4) approximating 1. While, the longitudinal direction remains phase-mismatched as expressed by the middle term.[31] The left term corresponds to the pure or spiral phase embedded cubic phase of SH Airy beam or AVB. When $\Gamma = (2n+1)\pi$ (n is an integer) via properly selecting the applied voltage (V) on the LC q-plate, OAM with $m_1 = 2q$ is loaded to the FW before illuminating on LN-Airy mask, and then SH AVB is generated with a doubled topological charge $m_2 = 4q$. For $\Gamma = 2n\pi$, FW remains Gaussian beam without phase modulation, and SH Airy beam is obtained in first diffraction orders. Therefore, through collaborating the binary mask engineered LN and spiral-variant geometric phase imprinted LC, the switchable SHG between Airy beam and AVB can be accomplished conveniently.

In experiment, the widely used electric-field poling method is employed to encoding the designed binary phase mask (Figure 1a) into the quadratic susceptibility distribution of LN crystal.[32] Firstly, a 120-nm-thick Cr patterned electrode is transformed on the $+z$ face of the 50-μm-thick z-cut LN slice through successive process of maskless photolithography, vacuum deposition, and photoresist removal. Then, by applying high voltage pulses of 1060 V (pulse period, 1s) which is slightly larger than the coercive field of used LN slice, the polarization directions of Cr-electrodes-covered LN domains are reversed, forming the designed LN-Airy mask. The fabricated domain structure can be vividly imaged by the SH confocal microscopy.[33] As exhibited in Figure 1e, domain walls of the engineered LN crystal can be obviously distinguished because of the opposite polarization direction of neighbor domains.

On the other hand, the photo-alignment technology[34–36] is introduced to fabricate the LC q-plate. Take one with $q = 0.5$ as an example, whose theoretical director distribution is shown in Figure 1b. Here, the sulfonic azo-dye SD1, a polarization-sensitive and rewritable alignment agent, is adopted. SD1 molecules tend to reorient perpendicular to the polarization direction of the illuminated UV light and further guide the LC directors. Two pieces of indium-tin-oxide glass substrates spin-coated with SD1 were assembled with 6-μm spacers and then sealed with epoxy glue to form the LC cell. Through a digital micro-mirror device based dynamic microlithography system, a multi-step partly-overlapping exposure process was performed to carry out the designed space-variant orientations.[37] Afterward, filling the patterned cell with nematic LC E7 yielded the LC q-plate. Figure 1f shows the experimental micrograph of the fabricated LC q-plate captured by a polarization microscope, where continuously changing brightness indicates the desired spiral-variant optical axes.

The schematic of experimental setup is exhibited in Figure 1i. The FW outputs from a Ti:sapphire femtosecond laser (Revolution, Coherent, USA) pumped optical parametrical amplifier (TOPAS-Prime, Light Conversion, Lithuania), and has a pulse width of 50 fs, a repetition rate of 1 kHz and an adopted wavelength of 1300 nm. The FW is spatially filtered, expanded, and collimated using two spherical lenses (f = 500 and 200 mm) combined with a pinhole at the Fourier plane of the 4f configuration. A sandwich configuration of a LC q-plate between two QWPs works as a switchable convertor between Gaussian beam and optical vortex. A short pass filter is used to block the rest of FW, and a spherical lens having f = 200 mm is employed to realize Fourier transformation of the nonlinear Airy beam and AVB. A charge coupled device (VTSE3S-2000, Vihent, China) is adopted to capture beam patterns. A voltage of V = 1.4 V is applied to the LC q-plate to satisfy the half-wave condition of FW (λ_{FW} = 1300 nm). FW becomes an optical vortex as captured in Figure 1c, whose topological charge is verified by the astigmatic transformation method based on a cylindrical lens (f = 100 mm).[30] As shown in Figure 1g, the number and tilt direction of dark stripes in the converted pattern indicate the value and sign of the topological charge, i.e., $m_1 = +1$. By illuminating such OAM imprinted FW onto the homogeneous domain of the same LN-Airy mask, nonlinear optical vortex is generated in the SHG process. The wavelength changes from invisible 1300 nm to red 650 nm, which can be directly distinguished in Figure 1d. Corresponding OAM detection with two dark

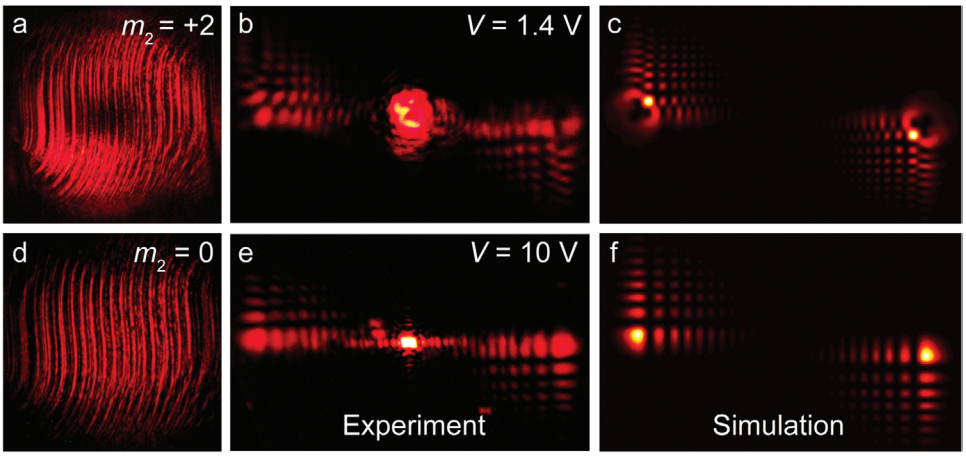

Figure 2. a,d) Second-harmonic (SH) beam patterns near the output surface of lithium niobate (LN) Airy mask, b,e) experimental results and c,f) theoretical calculations of SH Airy vortex beam (AVB) and Airy beam at the applied voltage $V = 1.4$ and 10 V, respectively.

stripes (Figure 1h) verifies a doubled topological charge ($m_2 = +2$), which matches well with theoretical prediction in Equation (4) and previous studies.[38,39]

Theoretical and experimental results of dynamic switching between SH Airy beam and AVB are exhibited in **Figure 2**. When FW at $V = 1.4$ V illuminates the LN-Airy mask, the SH beam pattern near the output surface is directly captured by a microscope system. The electric-poling induced domain walls of LN nonlinear photonic crystal and the doughnut shape of the SH optical vortex ($m_2 = +2$) can be clearly observed in Figure 2a. In this case, a pair of nonlinear AVBs with opposite propagation direction are generated simultaneously in first diffraction orders in the far field (Figure 2b). The main lobe of the SH AVB is split due to the OAM embedding. Except for the existence of zeroth order attributed to non-ideal conversion efficiency, experimental result shows a good consistence with the simulation (Figure 2c). When $V = 10$ V (i.e., Γ approaches 0), SH beam pattern transforms to a Gaussian profile as shown in Figure 2d, indicating a SHG without spiral phase modulation ($m_2 = 0$). Accordingly, far-field SH diffraction is switched to a pair of 2D Airy beams possessing complete main lobe and side lobes (Figure 2e), consistent with the simulation in Figure 2f. Therefore, through tuning the applied voltage, dynamic nonlinear wave-front engineering is demonstrated as desired. For the nematic LC material used here, the switching time is in the millisecond scale, which can be further improved to sub-millisecond and even tens of microsecond, by employing dual-frequency or ferroelectric LCs.[40] Moreover, thanks to the electro-optical tunability of LCs, the same LC q-plate can work at a wide wavelength range of the FW, making our scheme broadband available by adjusting the applied voltages.

What's more, the propagation dynamics of SH AVB is further analyzed in this nonlinear process, exhibiting a typical self-acceleration feature. Corresponding diffraction patterns are captured at different propagation distances with an interval of 5 cm away from the Fourier plane of the lens. The pair of SH AVBs in first orders bend in opposite transverse (x-) and longitudinal (y-) directions. Deflection in y-direction between two main lobes is measured as the criteria to conveniently and accurately characterize its propagation curving, as shown in **Figure 3**. Theoretically, such longitudinal deflection can be derived as $y = \lambda^2 z^2/(8\pi^2 d_0^3)$,[41] where λ is the SH wavelength, and d_0 assumes 103 µm determined by the optical setup in our experiment. Experimental propagation trajectory of SH AVB exhibits a parabolic curve and the deflection exceeds 800 µm after propagating 40 cm, matching well with the theoretical calculation. Since it is mainly determined by the scale of the generated Airy beam, much stronger deflection can be expected by a Fourier lens with smaller focal length.[42] Besides, SH AVBs have larger initial velocity in x-direction due to the existence of grating structure in LN-Airy mask, as vividly verified by the inserts in Figure 3. In the experiment, the nonlinear frequency conversion efficiency is measured as $6.22 \times 10^{-12}\%$ W^{-1}, which is consistent with some related previous works.[32,43] Such a small value is attributed to the unfulfilled complete phase-matching condition of the nonlinear Raman–Nath diffraction. To further improve the conversion efficiency, the nonlinear

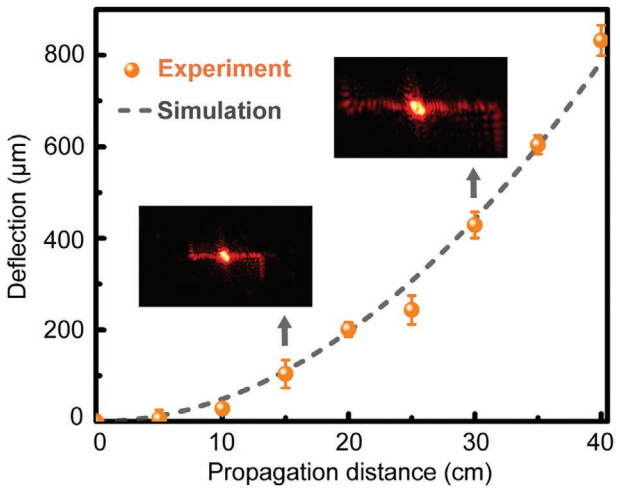

Figure 3. Dependency of the longitudinal deflection of generated second-harmonic (SH) Airy vortex beam (AVB) on the propagation distance. Yellow dots with error bars are experimental results, while gray dashed line is the simulated curve. Images captured at different distances are inserted near corresponding dots.

Bragg diffraction can be employed due to its full vectorial phase-matching scheme.[43,44] More recently, three-dimensional nonlinear photonic crystal has been demonstrated, whose effective conversion efficiency can be comparable to that of typical quasi phase-matching processes.[45]

In conclusion, dynamic switch between SH AVB and SH Airy beam is demonstrated. Electrically poled LN crystal is fabricated as a nonlinear Airy beam generator, whose nonlinear coefficients are modulated by a specific binary pattern. An electrical-switchable LC *q*-plate is further introduced to realize tunable OAM loading of the FW, resulting in the flexible SHG of AVB and Airy beam. Topological charge control, wavelength transformation, and curved propagation trajectory are achieved in one process. All experimental results are consistent with the theoretical prediction. The integration of space-variant anisotropic linear media and nonlinear photonic crystal will promote the dynamic nonlinear process and bring fantastic applications in optical manipulation and communication.

Acknowledgements

Y.L. and W.C. contributed equally to this work. This work was supported by the National Key Research and Development Program of China (No. 2017YFA0303700), the National Natural Science Foundation of China (NSFC) (Nos. 62035008, 12004175, 61922038, and 12004200), the Natural Science Foundation of Jiangsu Province (Nos. BK20180004 and BK20200311), the Fundamental Research Funds for the Central Universities (No. 021314380001), and the Innovation and Entrepreneurship Program of Jiangsu Province.

Conflict of Interest

The authors declare no conflict of interest.

Keywords

Airy beams, liquid crystals, nonlinear photonic crystals, vortex beams

Received: October 14, 2020
Revised: November 19, 2020
Published online: December 9, 2020

[1] A. Forbes, *Laser Photonics Rev.* **2019**, *13*, 1900140.
[2] M. V. Berry, N. L. Balazs, *Am. J. Phys.* **1979**, *47*, 264.
[3] G. A. Siviloglou, J. Broky, A. Dogariu, D. N. Christodoulides, *Phys. Rev. Lett.* **2007**, *99*, 213901.
[4] N. K. Efremidis, Z. Chen, M. Segev, D. N. Christodoulides, *Optica* **2019**, *6*, 686.
[5] Y. Guo, Y. Huang, X. Li, M. Pu, P. Gao, J. Jin, X. Ma, X. Luo, *Adv. Opt. Mater.* **2019**, *7*, 1900503.
[6] J. Baumgartl, M. Mazilu, K. Dholakia, *Nat. Photonics* **2008**, *2*, 675.
[7] A. Chong, W. H. Renninger, D. N. Christodoulides, F. W. Wise, *Nat. Photonics* **2010**, *4*, 103.
[8] T. Vettenburg, H. I. C. Dalgarno, J. Nylk, C. Coll-Llado, D. E. K. Ferrier, T. Cizmar, F. J. Gunn-Moore, K. Dholakia, *Nat. Methods* **2014**, *11*, 541.
[9] J. Wang, X. Hua, C. Guo, W. Liu, S. Jia, *Optica* **2020**, *7*, 790.
[10] L. Allen, M. W. Beijersbergen, R. J. C. Spreeuw, J. P. Woerdman, *Phys. Rev. A* **1992**, *45*, 8185.
[11] H. T. Dai, Y. J. Liu, D. Luo, X. W. Sun, *Opt. Lett.* **2011**, *36*, 1617.
[12] B. Wei, S. Qi, S. Liu, P. Li, Y. Zhang, L. Han, J. Zhong, W. Hu, Y. Lu, J. Zhao, *Opt. Express* **2019**, *27*, 18848.
[13] C. Xu, Y. Wu, D. Deng, *Opt. Lett.* **2020**, *45*, 3502.
[14] B. Y. Wei, S. Liu, P. Chen, S. X. Qi, Y. Zhang, W. Hu, Y. Q. Lu, J. L. Zhao, *Appl. Phys. Lett.* **2018**, *112*, 121101.
[15] B. K. Singh, R. Remez, Y. Tsur, A. Arie, *Opt. Lett.* **2015**, *40*, 5411.
[16] J. Zhou, Y. Liu, Y. Ke, H. Luo, S. Wen, *Opt. Lett.* **2015**, *40*, 3193.
[17] A. Shapira, L. Naor, A. Arie, *Sci. Bull.* **2015**, *60*, 1403.
[18] H. Liu, J. Li, X. Fang, X. Zhao, Y. Zheng, X. Chen, *Phys. Rev. A* **2017**, *96*, 023801.
[19] H. Li, H. Liu, X. Chen, *Opt. Express* **2017**, *25*, 28668.
[20] H. Liu, X. Zhao, H. Li, Y. Zheng, X. Chen, *Opt. Lett.* **2018**, *43*, 3236.
[21] X. Hu, Y. Zhang, S. Zhu, *Adv. Mater.* **2020**, *32*, 1903775.
[22] T. Ellenbogen, N. Voloch-Bloch, A. Ganany-Padowicz, A. Arie, *Nat. Photonics* **2009**, *3*, 395.
[23] X. H. Hong, B. Yang, C. Zhang, Y. Q. Qin, Y. Y. Zhu, *Phys. Rev. Lett.* **2014**, *113*, 163902.
[24] A. Libster-Hershko, S. Trajtenberg-Mills, A. Arie, *Opt. Lett.* **2015**, *40*, 1944.
[25] H. Li, H. Liu, X. Chen, *Opt. Express* **2018**, *26*, 21204.
[26] R. W. Boyd, *Nonlinear Optics*, Elsevier and Academic Press, London, UK **2008**.
[27] W. H. Lee, *Appl. Opt.* **1979**, *18*, 3661.
[28] L. Marrucci, C. Manzo, D. Paparo, *Phys. Rev. Lett.* **2006**, *96*, 163905.
[29] A. Rubano, F. Cardano, B. Piccirillo, L. Marrucci, *J. Opt. Soc. Am. B* **2019**, *36*, D70.
[30] P. Chen, S. J. Ge, W. Duan, B. Y. Wei, G. X. Cui, W. Hu, Y. Q. Lu, *ACS Photonics* **2017**, *4*, 1333.
[31] N. V. Bloch, K. Shemer, A. Shapira, R. Shiloh, I. Juwiler, A. Arie, *Phys. Rev. Lett.* **2012**, *108*, 233902.
[32] M. Y. Wang, J. Tang, H. J. Wang, Y. Ming, Y. Zhang, G. X. Cui, Y. Q. Lu, *Appl. Phys. Lett.* **2018**, *113*, 081105.
[33] X. Huang, D. Wei, Y. Wang, Y. Zhu, Y. Zhang, X. P. Hu, S. N. Zhu, M. Xiao, *J. Phys. D: Appl. Phys.* **2017**, *50*, 485105.
[34] P. Chen, L. L. Ma, W. Hu, Z. X. Shen, H. K. Bisoyi, S. B. Wu, S. J. Ge, Q. Li, Y. Q. Lu, *Nat. Commun.* **2019**, *10*, 2518.
[35] P. Chen, B. Y. Wei, W. Hu, Y. Q. Lu, *Adv. Mater.* **2020**, *32*, 1903665.
[36] H. Yu, M. Jiang, Y. Guo, T. Turiv, W. Lu, V. Ray, O. D. Lavrentovich, Q. H. Wei, *Adv. Opt. Mater.* **2019**, *7*, 1900117.
[37] P. Chen, B. Y. Wei, W. Ji, S. J. Ge, W. Hu, F. Xu, V. Chigrinov, Y. Q. Lu, *Photonics Res.* **2015**, *3*, 133.
[38] Z. Y. Zhou, S. L. Liu, Y. Li, D. S. Ding, W. Zhang, S. Shi, M. X. Dong, B. S. Shi, G. C. Guo, *Phys. Rev. Lett.* **2016**, *117*, 103601.
[39] X. Fang, Z. Kuang, P. Chen, H. Yang, Q. Li, W. Hu, Y. Lu, Y. Zhang, M. Xiao, *Opt. Lett.* **2017**, *42*, 4387.
[40] Y. Liu, P. Chen, R. Yuan, C. Q. Ma, Q. Guo, W. Duan, V. G. Chigrinov, W. Hu, Y. Q. Lu, *Opt. Express* **2019**, *27*, 36903.
[41] H. Wang, J. Du, H. Wang, Y. Lu, P. Wang, *Adv. Opt. Mater.* **2019**, *7*, 1900552.
[42] Z. Cai, Y. Liu, C. Zhang, J. Xu, S. Ji, J. Ni, J. Li, Y. Hu, D. Wu, J. Chu, *Opt. Lett.* **2017**, *42*, 2483.
[43] A. Shapira, R. Shiloh, I. Juwiler, A. Arie, *Opt. Lett.* **2012**, *37*, 2136.
[44] S. M. Saltiel, D. N. Neshev, W. Krolikowski, A. Arie, O. Bang, Y. S. Kivshar, *Opt. Lett.* **2009**, *34*, 848.
[45] D. Wei, C. Wang, H. Wang, X. Hu, D. Wei, X. Fang, Y. Zhang, D. Wu, Y. Hue, J. Lie, S. Zhu, M. Xiao, *Nat. Photonics* **2018**, *12*, 596.